Correlated response in a driven flow of self-organizing particles around a slit in porous media by interacting lattice gas

R. B. Pandey
Department of Physics and Astronomy, University of Southern Mississippi, Hattiesburg, Mississippi 39406, USA

J. F. Gettrust
50 Day Circuit, Bungendore, New South Wales 2621, Australia

(Received 25 February 2009; published 23 July 2009)

The flow of immiscible particles (A, B) through a porous medium with a vertical slit is studied by an interacting lattice-gas computer simulation on a discrete lattice. The source of the particles is connected to the bottom and particles are driven upward by concentration gradient and a pressure bias against gravity. Distribution of flowing particles around the slit is examined as a function of the slit width and bias at high and low porosity at a steady state. At the low bias, a sharp change in the densities (high in slit to low in adjacent porous media) of both constituents occurs as expected. Onset of an undershooting in the density and mobility of particle profiles appears at the interface of slit and the porous medium on increasing the bias, an unexpected correlated response. The competition between the faster flow in the slit and slower motion of the particles in the surrounding porous medium induces stronger correlations at higher bias; as a result, a well-defined density profile emerges with higher density in the porous matrix away from the slit interface. The range of correlation and therefore the response increases on increasing the bias. Lowering the porosity to near the percolation threshold leads to the onset of oscillation in the density profile and broadening of the mobility profile, a distinct difference from the response at high porosity.

DOI: 10.1103/PhysRevE.80.011130 PACS number(s): 05.40.−a, 05.60.−k, 05.65.+b, 07.05.Tp

I. INTRODUCTION

Seeping of gas and fluid particles through slits and other narrow and complex channels are common natural occurrences [1–5] as well as common phenomena in industrial waste disposal processes. Oil and natural gas seeps are natural geological processes [1–5] in which hydrocarbons in liquid and gas form and their various mixtures leak out of ground, the natural porous medium. For example, California [4] has cataloged seeps involving mixtures of crude oil, asphaltum (tar), natural gas, and water over the years in onshore and offshore areas. Abundant living communities (such as unusual tubeworms, mussels, and other creatures like those found at hydrothermal vents) consisting of microbial mats with methanotrophic bacteria have been found near methane seeps on the deep ocean floor [5,6]. Many of the seeps seem to occur through slits or fault openings driven by pressure gradients.

How the constituents flow through slits and disperse in surrounding media are the subjects of geological survey and field studies [6,7]. Identifying specific patterns and drawing meaningful and reliable conclusions [8,9] are often limited by the enormity of the parameters and variables such as the makeup of the media, variability in porosity, constituents of fluid mixtures and the various phases, and driving mechanisms such as density/concentration gradients, pressure, temperature, etc. The success of field measurements and surveys are often hindered due to the inability to control variables and parameters in naturally occurring processes and the resolution of the probing instruments. In such a complex scenario, one is left with intelligent guesses about the media, constituents, the driving mechanisms, and many "what if" questions. Computer simulation experiments with well-defined issues can be useful in simplifying complex parameters to gain more information from data; thus, it would be beneficial to develop a computer simulation model to probe the distribution of fluid around a slit in a random porous medium.

Flow and structural evolutions in many complex fluids including granular systems [10–12] have been extensively studied by coarse-grained particles covering a diverse variation in spatial and temporal scales. Examples include nanoscale material behavior in the laboratory, flow of fluid and sediment mixtures in geomarine environment, dissociation of methane and hydrocarbon below the ocean floor [6,8,9], eruption of mud volcanoes and settling of underlying constituents, etc. Computer simulations with particles are helpful to gain insight into the evolution of global patterns from the microscopic details. A number of lattice-gas methods [13–15] have been used to study flow in many such systems. However, it is easier to incorporate specific details such as interactions among constituent particles and the host medium in interacting lattice gas as in standard molecular dynamics [16–18] and Monte Carlo [19] methods to study both structural evolution and flow. In recent years, we have investigated the transport, flow, and distribution of self-organizing immiscible driven particles with the interacting lattice-gas model [20–22]. We extend the same model to study the mobility of the driven constituents and their dispersion in a porous medium with a uniform slit. The model is relatively simple and provides good insight into the responsive correlations in dispersion of flowing particles around the slit.

II. MODEL

We consider a heterogeneous lattice of size $L_x \times L_y \times L_z$ with a uniform slit of width L_s in the middle, i.e., the size of

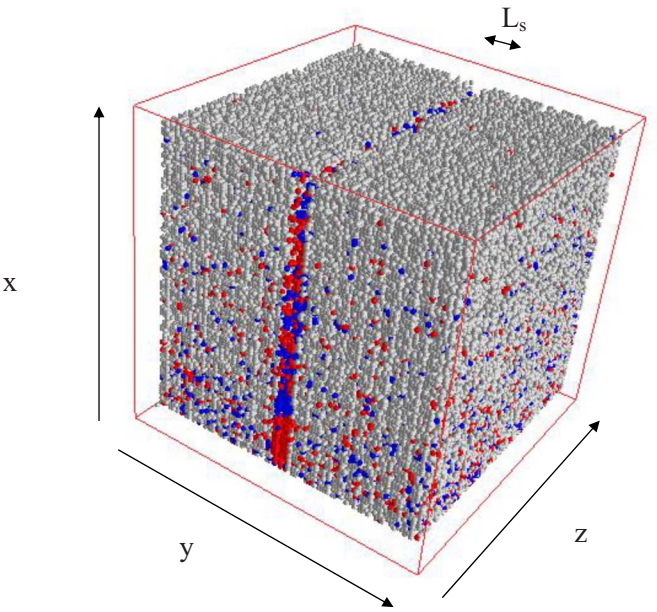

FIG. 1. (Color online) A typical porous medium with barrier sites (gray) and a slit in the middle. Distribution of immiscible particles A [blue (dark grey), $M_A=0.1$] and B [red (medium grey), $M_B=0.3$] with pressure bias $H=0.2$ at time steps $t=1000$ on an 80^3 lattice.

the slit is $L_x \times L_s \times L_z$. The overall matrix is a cubic lattice with $L_x=L_y=L_z=L$ with a narrow rectangular slit open across the center (Fig. 1). The heterogeneous porous matrix is generated by distributing immobile barriers (sediments) on a fraction p_b of the lattice sites (one barrier at a site) excluding the slit.

A source of a two-component fluid represented by mobile particles A and B with molecular weight $M_A=0.1$ and $M_B=0.3$, respectively, is connected to the bottom ($x=1$) of the lattice with the open top ($x=L_x$). Mobile particles A and B are randomly distributed initially at about 50% of the lattice sites with one particle at a site. A nearest-neighbor interaction between particles (A, B) and empty (pore) sites (O) is described by the energy

$$E_i = \sum_k \sum_n J(k,n), \tag{1}$$

where index k runs over all sites occupied by particles and n over all nearest-neighbor sites of k. The interaction matrix elements

$$J(A,A) = J(B,B) = -J(A,B) = -J(B,A) = J(A,O) = J(B,O) = -\varepsilon. \tag{2}$$

The interaction strength $\varepsilon=1$ is a measure of the miscibility gap between A and B. The gravitational potential energy, E_g, of a particle at height x (in units of g, the acceleration due to gravity) is given by

$$E_g = M_{A/B} x. \tag{3}$$

The sedimentation probability of A and B is coupled with the change in their gravitational potential energy via the Boltzmann distribution (see below). The concentration gradient caused by the source of particles at the bottom ($x=1$) exerts an upward driving force. Additionally, a bias H (pressure) pushes fluid constituents A and B upward ($+x$ direction) against the gravitational sedimentation downward ($-x$ direction). The bias is implemented in selecting the direction ($\pm x$, $\pm y$, and $\pm z$) of the moves of each particle to their nearest-neighbor sites with probabilities

$$P_x = (1+H)/6, \quad P_{-x} = (1-H)/6, \quad P_y = P_{-y} = P_z = P_{-z} = 1/6, \quad 0 \le H \le 1. \tag{4}$$

Movement of a particle is implemented by the following algorithm. A particle at a site, i, is selected randomly to move to one of its nearest-neighbor sites, j, selected with the bias probability H. If the site j is already occupied by another particle, then the attempt to move the particle fails. If the site j is empty, then the particle is moved (from the site i to site j) with the Boltzmann probability $\exp(-\Delta E/\tau)$, where ΔE is the change in energy $E=E_i+E_g$ due to the move and τ is the temperature in units of the Boltzmann constant and energy; $\tau=1$ is used in this study. As soon as a particle leaves the bottom plane ($x=1$) a new particle (A or B) from the source is released into the vacated site according to its current lattice concentration. The cubic box is open along vertical boundaries, i.e., a particle can drop out from the bottom or escape from the top ($x=L$). Periodic boundary conditions are implemented along the transverse (y and z) directions. An attempt to move each particle once defines unit Monte Carlo step (MCS) time. We keep track of such physical quantities as the root-mean-square displacement of each particle and the center of mass, density, and mobility profiles. The responses of density and mobility profiles to bias H are analyzed in detail around the slit as follows.

The parameters including the molecular weight (M_A and M_B) of particles A and B, temperature (τ), interaction energy among the constituents and the gravitational potential energy, and spatiotemporal variations in the physical quantities are in a nondimensional arbitrary form. Connecting such statistical models to a real system quantitatively (such basic units as meter, second, and Celsius for length, time and temperature) require calibration of the physical quantities and a relation between the interaction of the coarse-grained representation of particles and their atomic constituents. Such a calibration between the arbitrary units used here and the real spatiotemporal units and dimension is not feasible due to lack of field [5–7] and laboratory [23] measurements of a systematic variation in the physical quantities with appropriate parameters, e.g., seeping of methane gas as a function of pressure gradient below the ocean floor [7] and variation in fluid flux in a sediment sample [23] with the concentration of fluid mixture. However, the relative changes in response of such quantities as the density and mobility to pressure gradient and porosity can be predicted and compared qualitatively. This study with the idealized models may be useful to guide experiments (both field and laboratory) in assessing the trends.

III. RESULTS AND DISCUSSION

Simulations are performed for sufficiently long time steps to reach the steady state as the system is continuously driven

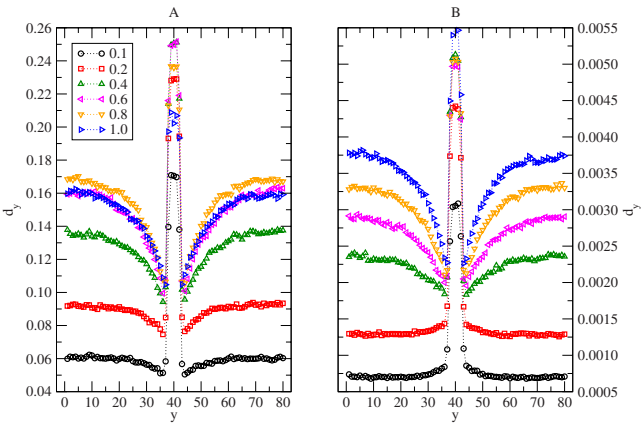

FIG. 2. (Color online) Transverse (y) density profile of particles A (M_A=0.1) and B (M_B=0.3) at pressure bias H=0.1–1.0 on an 80^3 lattice with slit of width L_s=5 surrounded by a heterogeneous medium with porosity p_s=0.5. One hundred independent samples are used to estimate the average density profiles.

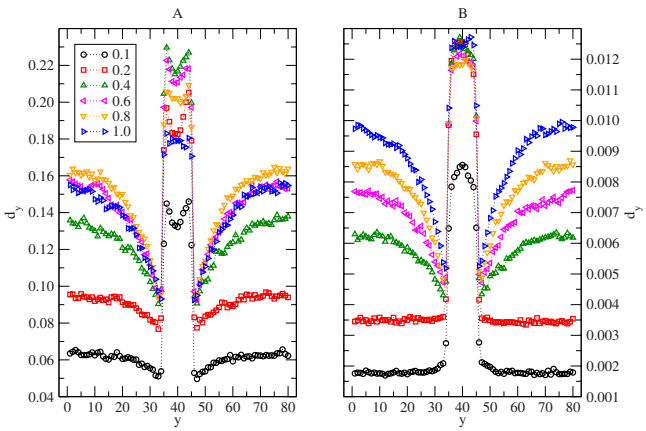

FIG. 3. (Color online) Transverse (y) density profile of particles A (M_A=0.1) and B (M_B=0.3) at pressure bias H=0.1–1.0 on an 80^3 lattice with slit of width L_s=10 surrounded by a heterogeneous medium with the porosity p_s=0.5. (Statistics are the same as Fig. 2.)

out of equilibrium. Different samples sizes are used to verify the finite-size effects and no severe finite-size effects are observed with the qualitative behavior of the physical quantities, e.g., the density profiles and mobility. Most of the simulations are performed on a 80^3 lattice with slit width L_s=5, 10, and 20 and porosity $p_s=(1-p_b)$=0.5 and 0.312, each with a number of independent samples. Note that the percolation threshold for the random percolating lattice is about 0.3117. It takes about five hours of CPU on a desktop computer for a typical data set and therefore the whole simulation is accessible to personal computing. Figure 1 shows the host matrix with a slit and a snap of mobile particles. Density profiles of particles (A and B) are evaluated to quantify their distributions. The planar density $[d_{x/y/z}(A/B)]$ is calculated from the number of corresponding particles (A or B) per unit area, e.g.,

$$d_i(A/B) = (1/L^2)\sum_{jk} \rho_{ijk}(A/B), \tag{5}$$

where the site occupancy $\rho_{ijk}(A/B)$=1 if the site (i, j, and k) is occupied by A/B particle and $\rho_{ijk}(A/B)$=0 otherwise.

The longitudinal (x) density profile involves averaging over the lattice sites in the yz planes, which contain sites from both slit and porous regions. As a result, it is difficult to distinguish the difference in particle densities in two regions. In general, the longitudinal density is higher at the bottom and low at the top in the steady state. The effect of the bias is clear with higher density at higher bias, but the effect of an open slit and its porous surroundings on the distribution of particles is less clear.

The effect of the heterogeneous matrix on the distribution of particles is more illustrative if we examine the transverse (y) profiles. Figures 2–4 show the transverse (y) density profiles with the slits of width L_s=5, 10, and 20 surrounded by the heterogeneous medium of porosity p_s=0.50. As expected, the density in slit region is higher due to open channels (i.e., porosity p_s=1) for mobile particles to flow through and the lower density in the surrounding regions with lower porosity. However, the response of the density profile pattern to bias is interesting. At low bias, e.g., H=0.1, the density of both A and B is nearly uniform in the surrounding regions. A careful examination of the density profiles of A and B shows a difference in their response near the slit: a somewhat opposite density gradient response at low values of bias (e.g., Fig. 2, H=0.1 and 0.2).

On increasing the bias, the profile responds systematically to a nonlinear form with the lowest value of density (depletion zone) at the interface of the slit and the surrounding pore. The minimum at the slit boundary followed by a radial increasing trend suggests the onset of correlation caused by the bias. The density gradient [slope of density versus distance (y), $\nabla_y d$] at the slit interface increases on increasing the bias and is a measure of correlation strength. The correlation decays with the decay of density gradient as a function of distance from the slit. One may think of the response correlation length as the range (distance) over which the density gradient becomes zero. This implies that the driven response correlation length increases on increasing the bias.

Let us look at the effects of the slit width and differences between the density profiles of A and B. There is a mono-

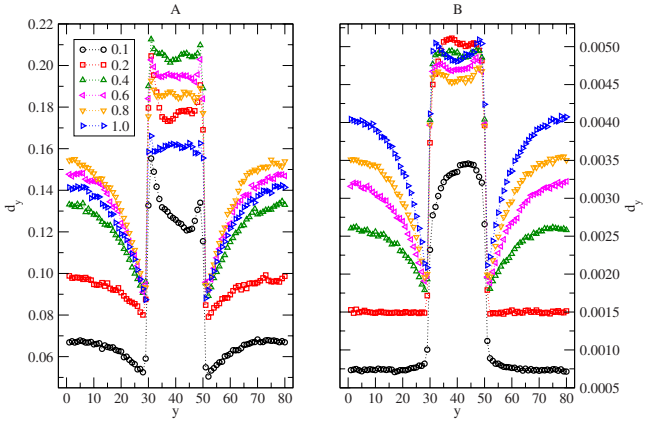

FIG. 4. (Color online) Transverse (y) density profile of particles A (M_A=0.1) and B (M_B=0.3) at pressure bias H=0.1–1.0 on an 80^3 lattice with slit of width L_s=20 surrounded by a heterogeneous medium with porosity p_s=0.5. (Statistics are the same as Fig. 2.)

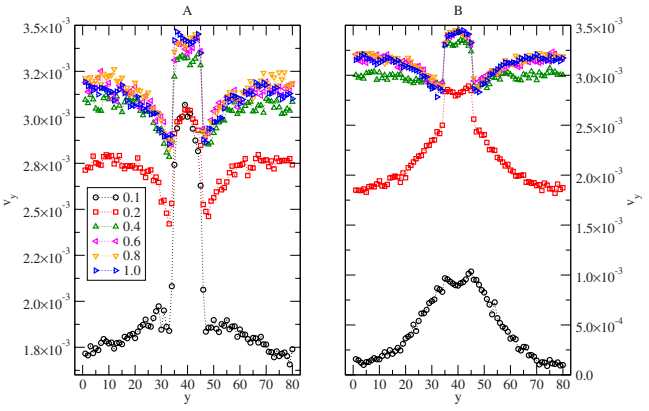

FIG. 5. (Color online) Velocity profile of particles A (M_A $=0.1$) and B ($M_B=0.3$) at pressure bias $H=0.1-1.0$ on an 80^3 lattice with slit of width $L_s=10$ surrounded by a heterogeneous medium with porosity $p_s=0.5$. (Statistics are the same as Fig. 2.)

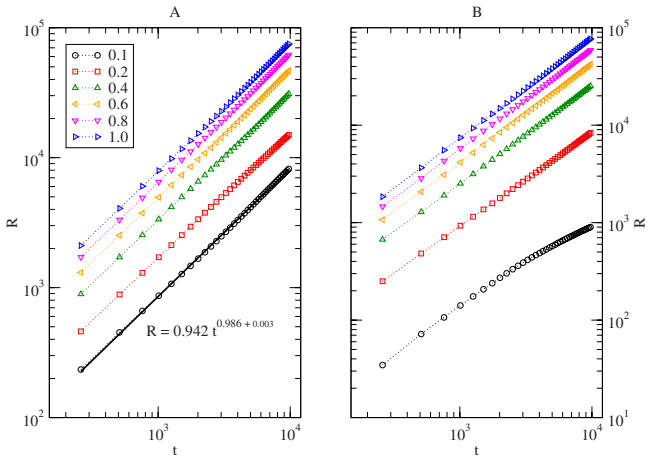

FIG. 6. (Color online) Variation in the root-mean-square displacement of each particle A ($M_A=0.1$) and B ($M_B=0.3$) with the time step on a log-log scale at pressure bias $H=0.1-1.0$ on an 80^3 lattice with slit of width $L_s=10$ surrounded by a heterogeneous medium with porosity $p_s=0.5$. (Statistics are the same as Fig. 2.)

tonic increase in the density gradient ($\nabla_y d$) of B, the higher molecular weight component, with the bias, which is less clear for A. Further, the response ($\nabla_y d$) at the slit interface also depends on the slit width, especially at low bias, e.g., $H=0.2$ for B (see Figs. 2–4). Flowing A and B are self-organizing and segregating, the complementarities in their density profiles are therefore expected, which is most feasible in the slit with the larger width (e.g., Fig. 4). This shows a clear phase separation of these immiscible components in the slit region. Note further, the nonmonotonic dependence of density with the bias (increase in density followed by decrease) in the slit (bulk) region is more clear for A in Fig. 4. The response of the density profile, thus, depends on the molecular weight of the mobile components and the size of the slit.

How fast do the constituents move as they flow through the open slit and the surrounding porous media? To estimate the local mobility, we evaluate the average speed (v), i.e., the distance traveled per unit time step since entering the lattice. From the velocity of each particle and their instantaneous position, one can track the mobility profile similarly to the density profile discussed above. Such a velocity profile is presented in Fig. 5. In general, the mobility profiles look similar to corresponding density profiles (see Fig. 3), e.g., the mobility is higher in the slit regions than in the surrounding pores. There are major differences, however, for example, at low bias ($H=0.1$ and 0.2), the mobility increases monotonically as particles move toward the slit from the heterogeneous porous bulk especially for the heavier component B with a somewhat sharp change at the interface. Increasing the bias ($H \geq 0.3$) leads to an undershooting of velocity at the interface of the slit followed by a sharp increase before reaching a steady state in the bulk (away from the slit). A systematic change in the response pattern of the velocity profile with the bias shows the onset of self-organized spatial velocity correlation similar to that seen in the density profiles.

A similar trend continues for the lighter component A at a somewhat lower bias (Fig. 5). For example, there is an increase in the velocity gradient at bias $H=0.1$ followed by a sharp increase with a correlated decay response away from the slit at bias $H \geq 0.2$. Apart from more fluctuations in the density profiles of A in comparison to that of B, the spatial trends in the responses of the mobility profiles are similar despite differences in their magnitudes.

On average, how each particle flows can be evaluated from the variation in the root-mean-square (RMS) displacement (R) of each particle (A and B) with the time steps. Figure 6 shows such a plot on a log-log scale. We see relatively good power-law dependence,

$$R = Ct^{\nu}, \tag{6}$$

with an exponent $\nu \approx 1$ which shows a drift motion for each particle. Apart from the slow motion of the heavier particles (B) at the low bias ($H=0.1$), both components show drift behavior at all biases. Drift is the signature of a driven motion; bias and concentration gradient drive the particles upward against gravity.

What happens when the porosity of the surrounding medium is reduced to a very low value, e.g., $p_s=0.312$, close to the percolation threshold, still spanning pathways of connected pores? Figure 7 shows the transverse density profiles of both particles A and B covering all ranges of bias ($H=0.0-1.0$). We see a dramatic change in density profiles in response to bias at the interface of the slit and the porous medium especially at high bias. The underpinning of density at the edge of the slit is followed by a sharp increase and then decrease as we move away from the slit; the onset of spatial oscillation in the density profile is more visible at H $=0.4-1.0$. Note that the response in the onset of the oscillatory density profile occurs at the porosity close to the percolation threshold in contrast to surroundings with higher porosity (compare Figs. 3 and 7). In the slit region, the density profiles of A and B seem complementary, suggesting the phase separation. The velocity profile at the porosity p_s $=0.312$ is presented in Fig. 8. The velocity profile appears much different from the corresponding density profile (Fig. 7). In contrast to the sharp undershoot at the slit boundary

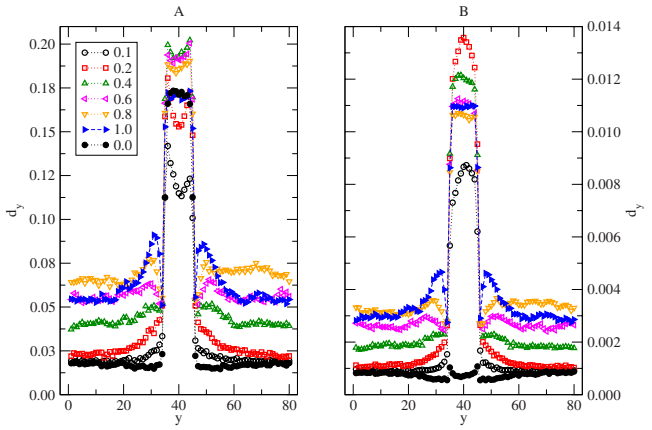

FIG. 7. (Color online) Transverse (y-) density profile of particles A (M_A=0.1) and B (M_B=0.3) at pressure bias H=0.1–1.0 on an 80^3 lattice with slit of width L_s=10 surrounded by a heterogeneous medium with porosity p_s=0.312. (Statistics are the same as Fig. 2.)

(Fig. 7), the density decreases gradually in the low porosity region. The decay of the density from its large value in the slit region broadens considerably in the low porosity surroundings as the width of the profile increases with the bias. Note further the contrast in response at high (p_s=0.5) and low (p_s=0.312) porosities: while the velocity profile (Fig. 5) follows the density profile (Fig. 3) at high porosity with an undershoot at the slit boundary at high bias, its decay smears out in the low porosity (Fig. 8). Correlation in the velocity profile seems to be damped down by more drag caused by more barriers at the low porosity. The variation in the RMS displacement of each particle with the time steps shows drift similar to those at high porosity (Fig. 5).

IV. CONCLUSIONS

An interacting lattice-gas model is used to study the distribution of a mixture of immiscible driven particles around a slit in porous media. The rectangular slit of width L_s (and size $L \times L_s \times L$) is in the middle of the host porous matrix on a cubic lattice. The porous medium of porosity p_s is generated by distributing immobile barriers randomly on a fraction $p_b = 1 - p_s$ of the lattice sites. A source of interacting particles (A and B) is connected at the bottom of the lattice with an open top. Particles, driven by a bias (H) and the concentration gradient, flow against gravity. The density and velocity of the particles reach steady state in the asymptotic time regime. Obviously, more particles flow through the open slit than the surrounding porous medium. How the particles distribute and move in and around the slit is examined by the computer simulations at porosity p_s=0.5 and 0.312 and bias H=0.0–1.0 with slit widths L_s=5, 10, and 20. Density and velocity profiles of constituents (A and B) are examined in the steady state.

The density profile and the velocity profile of both components depend on the porosity of the surrounding slit and the magnitude of the bias. The density and velocity of both particles are higher in the slit than in the surrounding porous region and the decay in the adjacent porous region depends on bias and porosity. The density profiles of A and B in the slit region are complementary exhibiting the segregation observed in a homogeneous system. At the high porosity (p_s =0.5), the velocity profiles and density profiles share similarities. The high density in the slit drops drastically and sharply at the slit boundaries but rebounds and grows as the particles move out into the surrounding porous medium. The rebound growth rate of density increases with increasing bias and becomes nonlinear with distance as particles move away from the slit. The velocity profiles exhibit somewhat similar patterns in response with some exceptions at low bias. The distribution of particles and their mobility seem more correlated as the bias competes with the pore barriers.

The response of the density and velocity profiles to bias is altered drastically on reducing the porosity to a low value (p_s=0.312) close to the percolation threshold. The density profiles exhibit the onset of oscillation beyond the drop at the edge of the slit, in contrast to the monotonic response at higher porosity. The percolation correlation length is relatively large for the surrounding porous media and the onset of oscillation in the correlated response of the density is due to interplay between bias and porosity. The velocity profiles show much different patterns than the corresponding density at low porosity in contrast to similarity in response observed at higher porosity. Not only does the velocity of the particles decreases at the interface of slit and the porous medium but also the width of its profile increases with the bias. In summary, the distribution of constituents and their mobility around the slit depend on the porosity of the surrounding medium and the driving bias. The response of the patterns in profile is sensitive to low porosity and high bias.

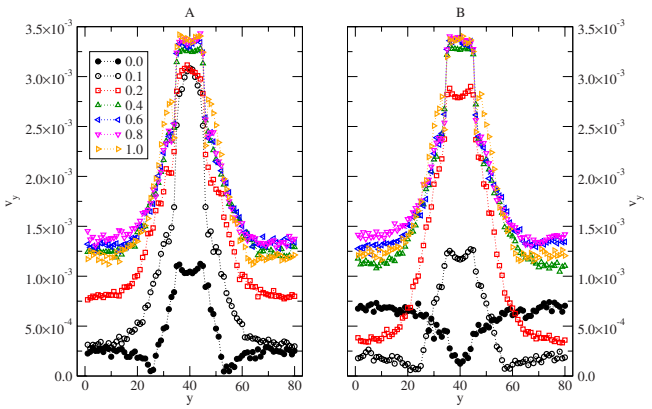

FIG. 8. (Color online) Velocity profile of particles A (M_A =0.1) and B (M_B=0.3) at pressure bias H=0.1–1.0 on an 80^3 lattice with slit of width L_s=10 surrounded by a heterogeneous medium with porosity p_s=0.312. (Statistics are the same as Fig. 2.)

ACKNOWLEDGMENTS

This work was done in part while the authors worked at the Naval Research Laboratory, Stennis Space Center, MS. We thank Diana B. Flosenzier for carefully reading and editing the manuscript.

[1] J. S. Hornafius, D. Quigley, and B. P. Luyenddyk, J. Geophys. Res. **104** (C9), 20703 (1999).
[2] L. Naudts, J. Greinert, Y. Artemov, P. Staelens, J. Poort, P. Van Rensbergen, and M. De Batist, Mar. Geol. **227**, 177 (2006).
[3] P. Eichhubl, H. G. Greene, T. Naehr, and N. Maher, J. Geochem. Exploration **69-70**, 545 (2000).
[4] Natural Oil and Gas Seeps in California (http://geomaps.wr.usgs.gov/seeps/).
[5] Biological communities near natural oil and gas seeps (http://www.mms.gov/omm/pacific/enviro/seeps2.htm).
[6] Proceedings of the Fourth International Conference on Gas Hydrate, Yokohama, 2002, (unpublished).
[7] W. T. Wood and J. F. Gettrust, in *Natural Gas Hydrates: Occurrence, Distribution, and Dynamics*, edited by C. K. Paull and W. P. Dillon, AGU Monograph No. 124 (2001), p. 165.
[8] Chuang Ji, G. Ahmadi, W. Zhang, and D. H. Smith, Proceedings of the Fourth International Conference on Gas Hydrate, Yokohama, 2002 (unpublished), p. 791.
[9] Hisashi O. Kono, B. Budhijanto, S. Narasimhan, and D. H. Smith, Proceedings of the Fourth International Conference on Gas Hydrate, Yokohama, 2002 (unpublished), p. 543.
[10] *Granular Matter: An Interdisciplinary Approach*, edited by A. Mehta (Springer, New York, 1994).
[11] *Unifying Concepts in Granular Media and Glasses*, edited by A. Coniglio, A. Fierro, H. J. Herrmann, and M. Nicodemi (Elsevier, New York, 2004).
[12] H. A. Makse, S. Havlin, P. R. King, and H. E. Stanley, in *Novel Pattern Formation in Granular Matter*, edited by L. Schimansky-Geier and T. Poeschel (Springer, Heidelberg, 1997), p. 319.
[13] D. H. Rothman and S. Zaleski, *Lattice-Gas Cellular Autoata Simple Models of Complex Hydrodynamics* (Cambridge University Press, Cambridge, 1997).
[14] D. A. Wolf-Gladrow, *Lattice Gas Cellular Automata and Lattice Boltzmann Models: An Introduction*, Lecture Notes in Mathematics (Springer, New York, 2000).
[15] S. Succi, *Lattice Boltzmann Equation for Fluid Dynamics and Beyond* (Oxford University Press, New York, 2001).
[16] D. C. Rapaport, Phys. Rev. E **65**, 061306 (2002).
[17] M. C. Mitchell, J. D. Autry, and T. M. Nenoff, Mol. Phys. **99**, 1831 (2001).
[18] G. Foffi, W. Gotze, F. Sciortino, P. Tartaglia, and Th. Voigtmann, Phys. Rev. E **69**, 011505 (2004).
[19] R. Finken, J. P. Hansen, and A. A. Louis, J. Phys. A **37**, 577 (2004).
[20] R. B. Pandey and J. F. Gettrust, Physica A **345**, 555 (2005).
[21] R. B. Pandey and J. F. Gettrust, Physica A **358**, 437 (2005).
[22] R. B. Pandey and J. F. Gettrust, Physica A **368**, 416 (2006).
[23] R. B. Pandey, A. H. Reed, E. Braithwaite, R. Seyfarth, and J. F. Gettrust, Physica A **374**, 501 (2007).